RAA 2017 Vol. **17** No. **7**, 66 (14pp) doi: 10.1088/1674–4527/17/7/66

http://www.raa-journal.org *http://iopscience.iop.org/raa*

***R**esearch in*
***A**stronomy and*
***A**strophysics*

The intrinsic γ-ray emissions of *Fermi* blazars

Chao Lin, Jun-Hui Fan† and Hu-Bing Xiao

Center for Astrophysics, Guangzhou University, Guangzhou 510006, China; *fjh@gzhu.edu.cn; linchao@e.gzhu.edu.cn*
Astronomy Science and Technology Research Laboratory of Department of Education of Guangdong Province, Guangzhou 510006, China

Received 2016 November 19; accepted 2017 March 17

Abstract The beaming effect is important for understanding the observational properties of blazars. In this work, we collect 91 *Fermi* blazars with available radio Doppler factors. γ-ray Doppler factors are estimated and compared with radio Doppler factors for some sources. The intrinsic (de-beamed) γ-ray flux density ($f_\gamma^{\rm in}$), intrinsic γ-ray luminosity ($L_\gamma^{\rm in}$) and intrinsic synchrotron peak frequency ($\nu_{\rm p}^{\rm in}$) are calculated. Then we study the correlations between $f_\gamma^{\rm in}$ and redshift and find that they follow the theoretical relation: $\log f = -2.0 \log z + {\rm const}$. When the subclasses are considered, we find that stationary jets are perhaps dominant in low synchrotron peaked blazars. Sixty-three *Fermi* blazars with both available short variability time scales (ΔT) and Doppler factors are also collected. We find that the intrinsic relationship between $L_\gamma^{\rm in}$ and $\Delta T^{\rm in}$ obeys the Elliot & Shapiro and Abramowicz & Nobili relations. Strong positive correlation between $f_\gamma^{\rm in}$ and $\nu_{\rm p}^{\rm in}$ is found, suggesting that synchrotron emissions are highly correlated with γ-ray emissions.

Key words: galaxies: active — BL Lacertae objects: general — gamma-rays: galaxies

1 INTRODUCTION

Two major subclasses of active galactic nuclei (AGNs) are radio loud AGNs and radio quiet AGNs. The radio-loud AGNs are blazars that have high and variable polarization, rapid and high amplitude variability, superluminal motions, strong γ-ray emissions, etc. Blazars have two subclasses, namely flat spectrum radio quasars (FSRQs) and BL Lacertae objects (BL Lacs). The difference between the two subclasses is mainly that BL Lacs show very weak (or even no) emission line features while FSRQs display strong emission lines. However, the continuum emission properties of BL Lacs and FSRQs are quite similar (Zhang & Fan 2003; Fan et al. 2009, 2014a; Xiao et al. 2015). BL Lacs were separately discovered through radio and X-ray surveys, and were divided into radio selected BL Lacs (RBLs) and X-ray selected BL Lacs (XBLs). From spectral energy distributions (SEDs), blazars can be divided into low synchrotron peaked (LSP, $\nu^s_{\rm peak} < 10^{14}\,$Hz), intermediate synchrotron peaked (ISP, $10^{14}\,{\rm Hz} < \nu^s_{\rm peak} < 10^{15}\,{\rm Hz}$), and high synchrotron peaked (HSP, $\nu^s_{\rm peak} > 10^{15}\,$Hz) blazars. This classification was first proposed by Abdo et al. (2010c) (see also Wu et al. 2007; Yang et al. 2014; Ackermann et al. 2015; Fan et al. 2015a; Lin & Fan 2016). In our recent work (Fan et al. 2016), a sample of 1392 *Fermi* blazars was collected, and their SEDs were obtained. Then, following the acronyms in Abdo et al. (2010c), we proposed classification by using the Bayesian classification method as follows: $\nu^{\rm s}_{\rm peak} < 10^{14}\,$Hz for LSP, $10^{14}\,{\rm Hz} < \nu^{\rm s}_{\rm peak} < 10^{15.3}\,{\rm Hz}$ for ISP, and $\nu^s_{\rm peak} > 10^{15.3}\,$Hz for HSP. We also pointed out that there are no ultra-HSP blazars (Fan et al. 2016).

Blazars have strong γ-ray emissions, and some of them even were detected in the TeV energy region (Weekes 1997; Catanese & Weekes 1999; Holder 2012; Xiong et al. 2013; Lin & Fan 2016). However, the origin of high energy emissions is still unclear. The *Fermi* Large Area Telescope (LAT) was launched in 2008, and detected many blazars at the γ-ray energy region (Abdo et al. 2010a; Nolan et al. 2012; Acero et al. 2015; Ackermann et al. 2015). Compared with its predecessor, the *Energetic Gamma Ray Experiment Telescope*

† Corresponding author.

(*EGRET*), the *Fermi*/LAT satellite has unprecedented sensitivity in the γ-ray band (Abdo et al. 2010c). The 3rd *Fermi* Large Area Telescope source catalog (3FGL) contains 3033 sources (see Acero et al. 2015), which gives us a large sample to analyze the mechanism of γ-ray emissions and other observed properties for blazars.

Beaming effect is included in the explanations of all electromagnetic emissions including γ-ray emissions for blazars, and many authors found that their γ-ray emissions have a strong beaming effect (e.g., Fan et al. 1999b, 2013b, 2014b; Fan & Ji 2014; Fan et al. 2015b; Fan 2005; Ruan et al. 2014; Chen et al. 2015, 2016; Cheng et al. 1999). Correlations are found between γ-ray emissions and other bands, and gamma-ray loud blazars are found to have larger Doppler factors than non-gamma-ray loud ones (Dondi & Ghisellini 1995; Valtaoja & Terasranta 1995; Xie et al. 1997; Fan et al. 1998; Cheng et al. 2000; Jorstad et al. 2001a,b; Lähteenmäki & Valtaoja 2003; Kellermann et al. 2004; Lister et al. 2009; Savolainen et al. 2010; Zhang et al. 2012; Li et al. 2013; Xiong et al. 2013; Wu et al. 2014; Xiao et al. 2015; Chen et al. 2016; Pei et al. 2016).

In a beaming model, the relativistic jet emissions are boosted such that $f^{\rm ob} = \delta^q f^{\rm in}$, where $f^{\rm in}$ is the intrinsic (de-beamed) emissions in the source rest frame, δ is a Doppler boosting factor and q depends on the shape of the jet: $q = 2 + \alpha$ for a stationary jet, $q = 3 + \alpha$ for a jet with distinct "blobs," and α is an energy spectral index ($f_\nu \propto \nu^{-\alpha}$). The Doppler boosting factor, which is defined as $\delta = [\Gamma(1 - \beta\cos\theta)]^{-1}$, is important for investigating the intrinsic properties of blazars. But it depends on two unobservable factors: the bulk Lorentz factor, $\Gamma = (1 - \beta^2)^{-1/2}$, and the viewing angle, θ, where β is the jet speed in units of the speed of light (see Fan et al. 2009; Savolainen et al. 2010).

Some methods are proposed to estimate the Doppler factors. Ghisellini et al. (1993) gave a method of estimating the Doppler factors, which was based on the synchrotron self-Compton model. This method assumes the X-ray flux originates from the self-Compton components, so a predicted X-ray flux can be calculated by using *Very Long Baseline Interferometry* (*VLBI*) data. By comparing this to the observed X-ray flux, the Doppler boosting factors can be calculated. After that, Lähteenmäki & Valtaoja (1999, hereafter LV99) proposed a more accurate and reliable method: the variability brightness temperature of the source ($T_{\rm b}^{\rm ob}$) obtained from the variability of VLBI data is used to compare with intrinsic brightness temperature of the source ($T_{\rm b}^{\rm in}$). $T_{\rm b}^{\rm in}$ is assumed to be the equipartition brightness temperature ($T_{\rm b}^{\rm eq}$), namely $T_{\rm b}^{\rm in} = T_{\rm b}^{\rm eq} = 5 \times 10^{10}$ K. So, the Doppler factor can be estimated by using $\delta = (T_{\rm b}^{\rm ob}/T_{\rm b}^{\rm in})^{1/3}$. When the variability time scales are obtained from total flux density observation, the variability brightness temperature can be calculated by using exponential flares and the variability time scales (LV99, see also Fan et al. 2009; Hovatta et al. 2009).

Because of short term variability, a highly compact engine exists at the center of blazars. The balance between gravitation and radiation pressure determines an upper limit of luminosity, namely Eddington luminosity, for any AGN (Bassani et al. 1983). If the short variability time scale is assumed to be equal to or greater than the time that light travels across the Schwarzschild radius of a black hole, then the observed luminosity and short variability time scale should obey the so called Elliot & Shapiro Relation (E-S Relation):

$$\log L \leq 43.1 + \log \Delta T$$

(Elliot & Shapiro 1974), where L is luminosity in units of erg s^{-1}, and ΔT is variability time scale in units of second (s). Generally, a short variability time scale is assumed to be a time scale which is shorter than one week (Fan 2005). When the anisotropy of emissions is considered, the above limit is replaced by the Abramowicz & Nobili Relation (A-N Relation):

$$\log L \leq 44.3 + \log \Delta T$$

(Abramowicz & Nobili 1982).

Intrinsic properties are required to analyze the origin of γ-ray emissions for blazars. In our recent work of Xiao et al. (2015), we considered the beaming effect of *Fermi* blazars in Nolan et al. (2012) (2FGL), then analyzed the correlation between γ-ray flux density and redshift for 73 blazars, and the relation between γ-ray short variability time scale and γ-ray luminosity by comparing with the E-S Relation and the A-N Relation for 28 blazars. In this work, we use a larger sample to revisit the relation between γ-ray flux density and redshift, and the relation between γ-ray luminosity and short variability time scale. The subclasses of blazars, and the short variability time scale from X-ray and optical bands are also considered. Then we have 91 *Fermi* blazars with available radio Doppler factors and 63 *Fermi* blazars with both available short variability time scales and Doppler factors. γ-ray Doppler factors are estimated for the *Fermi* blazars with available short variability time scales at optical, X-ray or γ-ray bands. In addition, the correlation between γ-ray emissions and synchrotron peaked frequency is also studied in this work.

This work is arranged as follows: we will describe our sample and corresponding results in Section 2, and give some discussions and conclusions in Section 3.

2 SAMPLE AND RESULTS

2.1 Sample

In this work, we collect blazars with available radio Doppler factors from the literature: LV99, Fan et al. (2009), Hovatta et al. (2009) and Savolainen et al. (2010). These references used the same method introduced by LV99. If the Doppler factors of some sources are available in more than one reference, we choose the value from the latest paper. Based on the third catalog of AGNs detected by the Fermi Large Area Telescope (3LAC) [1] (Ackermann et al. 2015), we collect a sample of 91 *Fermi* blazars with available radio Doppler factors, which are listed in Table 1.

In Table 1, γ-ray data are from 3LAC, and only the entry for PKS 2145+06 is from 2LAC [2] (Ackermann et al. 2011).

We derive the *Fermi* integral photon flux at 1–100 GeV, as we did in our previous works (Fan et al. 2013b, 2014b), and let

$$\frac{dN}{dE} = N_0 E^{-\alpha^{\rm ph}},$$

where $\alpha^{\rm ph}$ is a photon spectral index and $\alpha^{\rm ph} = \alpha - 1$. Then the flux density at energy E_0 in units of $\rm GeV\,cm^{-2}\,s^{-1}\,GeV^{-1}$ can be expressed as

$$f_E = \frac{N_{(E_{\rm L}\sim E_{\rm U})}(1-\alpha^{\rm ph})}{E_{\rm U}^{1-\alpha^{\rm ph}} - E_{\rm L}^{1-\alpha^{\rm ph}}} \cdot E_0^{1-\alpha^{\rm ph}}, \quad (1)$$

where $N_{(E_{\rm L}\sim E_{\rm U})}$ is photon flux in units of $\rm ph\,cm^{-2}\,s^{-1}$ in the energy range of $E_{\rm L} \sim E_{\rm U}$. Because the integral flux in $\rm GeV\,cm^{-2}\,s^{-1}$ can be obtained by $F = \int_{E_{\rm L}}^{E_{\rm U}} E dN = \int_{E_{\rm L}}^{E_{\rm U}} f_E dE$,

$$F = \frac{N_{(E_{\rm L}\sim E_{\rm U})} E_{\rm U} \times E_{\rm L}}{E_{\rm U} - E_{\rm L}} \ln\left(\frac{E_{\rm U}}{E_{\rm L}}\right), \quad \text{for } \alpha^{\rm ph} = 2$$

$$F = N_{(E_{\rm L}\sim E_{\rm U})} \frac{1-\alpha^{\rm ph}}{2-\alpha^{\rm ph}} \frac{\left(E_{\rm U}^{2-\alpha^{\rm ph}} - E_{\rm L}^{2-\alpha^{\rm ph}}\right)}{(E_{\rm U}^{1-\alpha^{\rm ph}} - E_{\rm L}^{1-\alpha^{\rm ph}})}, \quad \text{otherwise.} \quad (2)$$

For the *Fermi* sources in this work, $E_{\rm L}$ and $E_{\rm U}$ correspond to 1 GeV and 100 GeV respectively.

The synchrotron peak frequency ($\log \nu_{\rm p}^{\rm s}$) of PKS 2145+06 is not available in Fan et al. (2016) or 2LAC. We use the empirical relationship introduced in Fan et al. (2016) to estimate it as follows

$$\log \nu_{\rm p}^{\rm s} = \begin{cases} 16 + 4.238X & X < 0, \\ 16 + 4.005Y & X > 0, \end{cases} \quad (3)$$

where $X = 1 - 1.262\alpha_{\rm RO} - 0.623\alpha_{\rm OX}$, $Y = 1.0 + 0.034\alpha_{\rm RO} - 0.978\alpha_{\rm OX}$ (Fan et al. 2016), and $\alpha_{\rm RO}$ and $\alpha_{\rm OX}$ are the effective spectral indexes. For PKS 2145+06, we can get $\alpha_{\rm RO} = 0.666$ and $\alpha_{\rm OX} = 1.283$ from 2LAC, so we obtain $\log \nu_{\rm p}^{s} = 13.29$ Hz.

2.2 γ-ray Flux Density and Redshift

Our sample in Table 1 contains 32 BL Lacs and 59 FSRQs, or 40 ISP and 51 LSP based on the SED classification in Fan et al. (2016). In this work, we transform the γ-ray photon flux at 1–100 GeV into the flux density in units of mJy at $E_0 = 2$ GeV by using Equation (1), and apply separate linear regressions to the correlation between flux density and redshift for the whole sample, BL Lacs, FSRQs, ISP and LSP. All the fluxes are K-corrected by using $f = f^{\rm obs}(1+z)^{\alpha-1}$.

Whole sample: For the whole sample of 91 blazars, we have

$$\log f_\gamma = -(0.01 \pm 0.15)\log z - (8.96 \pm 0.06)$$

with a correlation coefficient $r = -0.01$ and a chance probability $p = 93.08\%$. As we introduce in Section 1, we can calculate the intrinsic flux density, then we have

$$\log f_\gamma^{\rm in} = -(1.82 \pm 0.30)\log z - (12.44 \pm 0.13)$$

with $r = -0.54$ and $p = 2.98 \times 10^{-8}$ for the case of $q = 2 + \alpha$, and

$$\log f_\gamma^{\rm in} = -(2.32 \pm 0.37)\log z - (13.46 \pm 0.16)$$

with $r = -0.55$ and $p = 1.66 \times 10^{-8}$ for $q = 3 + \alpha$. The corresponding figure is shown in Figure 1.

BL Lacs: For the 32 BL Lacs, we have

$$\log f_\gamma = -(0.13 \pm 0.24)\log z - (9.05 \pm 0.13)$$

with $r = -0.10$ and $p = 59.96\%$;

$$\log f_\gamma^{\rm in} = -(1.30 \pm 0.47)\log z - (11.82 \pm 0.26)$$

with $r = -0.45$ and $p = 1.03\%$ for $q = 2 + \alpha$; and

$$\log f_\gamma^{\rm in} = -(1.65 \pm 0.61)\log z - (12.68 \pm 0.34)$$

with $r = -0.44$ and $p = 1.13\%$ for $q = 3 + \alpha$. The corresponding figure is shown in the upper panel of Figure 2

FSRQs: For the 59 FSRQs, we have

$$\log f_\gamma = -(0.02 \pm 0.23)\log z - (8.94 \pm 0.07)$$

with $r = -0.01$ and $p = 94.20\%$;

$$\log f_\gamma^{\rm in} = -(1.34 \pm 0.45)\log z - (12.61 \pm 0.14)$$

[1] *http://www.asdc.asi.it/fermi3lac/*

[2] *http://www.asdc.asi.it/fermi2lac/*

Table 1 Sample of 91 *Fermi* Blazars

3FGL name	Other name	z	$\log \nu_{\rm p}^{\rm s}$	Class	$f_{\rm 2GeV}$	$\alpha_\gamma^{\rm ph}$	$\delta_{\rm R}$	Reference
(1)	(2)	(3)	(4)	(5)	(6)	(7)	(8)	(9)
J0050.6–0929	PKS 0048–09	0.300	14.60	IPB	12.67	2.09	9.6	H09
J0102.8+5825	TXS 0059+581	0.643	12.73*	LPQ	24.44	2.25	10.91	F09
J0108.7+0134	PKS 0106+01	2.099	13.53	IPQ	28.83	2.39	18.2	S10
J0112.1+2245	RX J0112.0+2244	0.265	14.39	IPB	29.55	2.03	9.1	S10
J0137.0+4752	S4 0133+47	0.859	12.69	LPQ	21.08	2.27	20.5	S10
J0151.6+2205	PKS 0149+21	1.320	13.14	LPQ	2.21	2.65	4.72	LV99
J0205.0+1510	4C +15.05	0.405	12.10	LPQ	2.82	2.53	15.0	S10
J0217.5+7349	S5 0212+73	2.367	13.35	LPQ	7.72	2.91	8.4	S10
J0217.8+0143	PKS 0215+015	1.721	14.66	IPQ	17.03	2.19	5.61	F09
J0222.6+4301	3C 66A	0.444	14.76	IPB	62.03	1.94	2.6	H09
J0237.9+2848	B2 0234+28	1.207	13.59	LPQ	45.20	2.35	16.0	S10
J0238.6+1636	PKS 0235+164	0.940	13.24	LPB	39.92	2.17	23.8	S10
J0303.6+4716	4C +47.08	0.475	14.10	IPB	8.89	2.28	4.33	F09
J0309.0+1029	PKS 0306+102	0.863	14.04	IPQ	11.18	2.23	2.79	F09
J0336.5+3210	B2 0333+32	1.259	13.55	LPQ	5.26	2.89	22.0	S10
J0339.5–0146	PKS 0336–01	0.852	13.40	LPQ	15.32	2.42	17.2	S10
J0423.2–0119	PKS 0420–01	0.915	12.88	LPQ	23.83	2.30	19.7	S10
J0424.7+0035	PKS 0422+00	1.025	14.22	IPB	7.45	2.20	6.11	F09
J0442.6–0017	PKS 0440–00	0.844	13.04*	LPQ	16.65	2.50	12.9	H09
J0449.0+1121	PKS 0446+11	1.207	13.09	LPQ	15.07	2.55	4.90	LV99
J0501.2–0157	PKS 0458–02	2.286	13.50	IPQ	13.33	2.41	15.7	S10
J0522.9–3628	PKS 0521–36	0.055	13.75	LPQ	17.06	2.44	1.83	F09
J0530.8+1330	PKS 0528+134	2.070	12.53	LPQ	22.96	2.51	30.9	S10
J0608.0–0835	PKS 0605–08	0.872	13.88	IPQ	9.27	2.37	7.5	S10
J0721.9+7120	1H 0717+714	0.310	14.96	IPB	75.14	2.04	10.8	S10
J0725.8–0054	PKS 0723–008	0.127	14.00	IPB	3.93	2.19	2.50	LV99
J0738.1+1741	PKS 0735+17	0.424	14.23	IPB	18.41	2.01	3.92	F09
J0739.4+0137	PKS 0736+01	0.191	14.43	IPQ	10.46	2.48	8.5	S10
J0757.0+0956	PKS 0754+100	0.266	14.05	IPB	6.71	2.18	5.5	S10
J0807.9+4946	S4 0804+49	1.436	13.28	LPQ	1.60	2.57	35.2	S10
J0811.3+0146	OJ 014	0.407	13.28	LPB	8.97	2.16	5.39	F09
J0818.2+4223	B3 0814+425	0.245	13.52	LPB	22.22	2.11	4.6	S10
J0820.9–1258	PKS 0818-128	0.407	14.77	IPB	1.03	2.27	3.18	F09
J0830.7+2408	B2 0827+24	0.941	13.50	LPQ	5.79	2.63	13.0	S10
J0831.9+0430	PKS 0829+046	0.230	13.84	LPB	12.43	2.24	3.80	F09
J0841.4+7053	RBS 0717	2.218	14.44	IPQ	11.43	2.84	16.1	S10
J0849.9+5108	SBS 0846+513	1.860	13.36*	LPB	8.79	2.28	6.40	LV99
J0850.2–1214	PMN J0850–1213	0.566	13.10	LPQ	0.27	0.11	16.5	H09
J0854.8+2006	PKS 0851+202	0.306	14.21	IPB	21.46	2.18	16.8	S10
J0948.6+4041	B3 0945+408	1.249	13.86	IPQ	1.81	2.67	6.3	S10
J0956.6+2515	OK 290	0.712	13.98	IPQ	3.95	2.44	4.3	H09
J0957.6+5523	4C +55.17	0.901	14.74	IPQ	34.97	2.00	4.63	LV99
J0958.6+6534	S4 0954+65	0.367	14.02	IPB	5.47	2.38	5.93	F09
J1037.0–2934	PKS 1034-293	0.312	13.92	IPQ	2.03	2.49	2.80	F09
J1058.5+0133	PKS 1055+01	0.888	13.79	IPQ	25.88	2.21	12.1	S10
J1129.9–1446	PKS 1127–14	1.187	13.99	IPQ	5.69	2.79	3.22	F09
J1159.5+2914	B2 1156+29	0.729	13.04	LPQ	32.64	2.21	28.2	S10
J1221.4+2814	W Comae	0.102	14.83	IPB	14.24	2.10	1.2	H09
J1224.9+2122	PG 1222+216	0.432	14.53	IPQ	99.31	2.29	5.2	S10
J1229.1+0202	PKS 1226+02	0.158	15.12	IPQ	36.15	2.66	16.8	S10
J1256.1–0547	3C 279	0.536	12.69	LPQ	83.67	2.34	23.8	S10
J1309.5+1154	PKS 1307+121	0.407	13.72	LPB	2.12	2.14	1.22	F09
J1310.6+3222	B2 1308+32	0.997	13.22	LPQ	15.17	2.25	15.3	S10
J1326.8+2211	B2 1324+22	1.400	12.97	LPQ	8.64	2.45	21.0	S10
J1337.6–1257	PKS 1335–12	0.539	13.25	LPQ	6.63	2.44	8.3	S10

Table 1 — *Continued.*

3FGL name	Other name	z	$\log \nu_{\rm p}^{\rm s}$	Class	$f_{\rm 2GeV}$	$\alpha_\gamma^{\rm ph}$	$\delta_{\rm R}$	Reference
(1)	(2)	(3)	(4)	(5)	(6)	(7)	(8)	(9)
J1408.8–0751	PKS B1406–076	1.494	12.86	LPQ	8.91	2.38	8.26	LV99
J1416.0+1325	PKS 1413+135	0.247	12.57	LPB	2.02	2.36	12.1	S10
J1419.9+5425	OQ 530	0.151	14.27	IPB	3.53	2.31	2.79	F09
J1504.4+1029	PKS 1502+106	1.839	13.34	LPQ	107.57	2.24	11.9	S10
J1512.8–0906	PKS 1510–089	0.360	13.97	IPQ	161.49	2.36	16.5	S10
J1540.8+1449	PKS 1538+149	0.605	13.97	IPB	1.53	2.34	4.3	S10
J1608.6+1029	PKS 1606+10	1.226	13.39	LPQ	7.41	2.62	24.8	S10
J1613.8+3410	B2 1611+34	1.397	13.44	LPQ	3.11	2.35	13.6	S10
J1635.2+3809	B3 1633+382	1.814	13.21	LPQ	60.94	2.40	21.3	S10
J1637.9+5719	S4 1637+57	0.751	14.22	IPQ	1.53	2.81	13.9	S10
J1642.9+3950	3C 345	0.593	13.46	LPQ	10.90	2.45	7.7	S10
J1719.2+1744	PKS 1717+177	0.407	13.91	IPB	5.43	2.04	1.94	F09
J1728.5+0428	PKS 1725+044	0.293	13.32	LPQ	3.65	2.59	3.8	H09
J1733.0–1305	PKS 1730–130	0.902	12.62	LPQ	24.61	2.35	10.6	S10
J1740.3+5211	S4 1739+52	1.379	13.42	LPQ	8.66	2.45	26.3	S10
J1744.3–0353	PKS 1741–03	1.054	14.06	IPQ	2.70	2.27	19.5	S10
J1748.6+7005	S4 1749+70	0.770	14.27	IPB	14.58	2.06	3.75	F09
J1751.5+0939	PKS 1749+096	0.322	12.99	LPB	15.92	2.25	11.9	S10
J1800.5+7827	S5 1803+78	0.684	13.90	IPB	19.78	2.22	12.1	S10
J1806.7+6949	3C 371	0.051	14.60	IPB	11.80	2.23	1.1	S10
J1824.2+5649	S4 1823+56	0.664	13.25	LPB	8.95	2.46	6.3	S10
J1829.6+4844	S4 1828+48	0.692	13.04*	LPQ	6.38	2.37	5.6	S10
J1924.8-2914	PKS B1921–293	0.352	12.53	LPQ	8.84	2.50	9.51	F09
J2005.2+7752	S5 2007+77	0.342	13.55	LPB	6.65	2.22	4.68	F09
J2123.6+0533	PKS 2121+053	1.941	13.40	LPQ	2.02	2.17	15.2	S10
J2134.1–0152	PKS 2131–021	1.285	13.17	LPB	4.62	2.21	7.00	F09
J2147.2+0929	PKS 2144+092	1.113	13.87	IPQ	12.93	2.54	5.96	LV99
J2148.2+0659	PKS 2145+06	0.990	13.29	LPQ	2.30	2.77	15.5	S10
J2158.0–1501	PKS 2155–152	0.672	13.09	LPQ	4.27	2.27	2.31	F09
J2202.7+4217	B3 2200+420	0.069	15.10	IPB	58.52	2.25	7.2	S10
J2203.7+3143	S3 2201+31	0.295	14.43	IPQ	0.89	3.07	6.6	S10
J2225.8–0454	3C 446	1.404	13.24	LPQ	9.37	2.36	15.9	S10
J2229.7–0833	PKS 2227–088	1.562	13.34	LPQ	20.79	2.55	15.8	S10
J2232.5+1143	PKS 2230+11	1.037	13.65	LPQ	25.54	2.52	15.5	S10
J2236.3+2829	B2 2234+28A	0.795	12.88	LPB	17.70	2.28	6.0	H09
J2254.0+1608	PKS 2251+15	0.859	13.54	LPQ	463.39	2.35	32.9	S10

Notes: Column (1) gives the *Fermi* name; Col. (2) other name; Col. (3) redshift (z); Col. (4) synchrotron peak frequency ($\log \nu_{\rm p}^{\rm s}$) in units of Hz from Fan et al. (2016), the data with "$*$" are from 3LAC; Col. (5) the classification, which depends on the peak frequency of the sources in the rest frame: $\nu_{\rm p}^{\rm res} = (1+z)\nu_{\rm p}^{\rm obs}$, "IPQ" for ISP FSRQs, "LPQ" for LSP FSRQs, "IPB" for ISP BL Lacs, "LPB" for LSP BL Lacs; Col. (6) γ-ray flux density at 2 GeV in units of 10^{-10} mJy; Col. (7) the γ-ray photon spectral index ($\alpha_\gamma^{\rm ph}$); Col. (8) radio Doppler factor ($\delta_{\rm R}$); Col. (9) references for Col. (8). Here, F09: Fan et al. (2009); H09: Hovatta et al. (2009); LV99: Lähteenmäki & Valtaoja (1999); S10: Savolainen et al. (2010).

with $r = -0.37$ and $p = 3.90 \times 10^{-3}$ for $q = 2+\alpha$; and

$$\log f_\gamma^{\rm in} = -(1.73 \pm 0.55)\log z - (13.68 \pm 0.17)$$

with $r = -0.39$ and $p = 2.50 \times 10^{-3}$ for $q = 3+\alpha$. The corresponding figure is shown in the lower panel of Figure 2.

ISP: For the 40 ISP blazars, we have

$$\log f_\gamma = -(0.12 \pm 0.22)\log z - (9.02 \pm 0.11)$$

with $r = -0.09$ and $p = 58.81\%$;

$$\log f_\gamma^{\rm in} = -(1.33 \pm 0.44)\log z - (12.01 \pm 0.22)$$

with $r = -0.44$ and $p = 4.12 \times 10^{-3}$ for $q = 2+\alpha$; and

$$\log f_\gamma^{\rm in} = -(1.67 \pm 0.54)\log z - (12.89 \pm 0.27)$$

with $r = -0.45$ and $p = 3.66 \times 10^{-3}$ for $q = 3+\alpha$. The corresponding figure is shown in the upper panel of Figure 3.

LSP: For the 51 LSP blazars, we have

$$\log f_\gamma = (0.09 \pm 0.22)\log z - (8.94 \pm 0.07)$$

with $r = 0.06$ and $p = 68.03\%$;

$$\log f_\gamma^{\rm in} = -(1.95 \pm 0.44)\log z - (12.66 \pm 0.14)$$

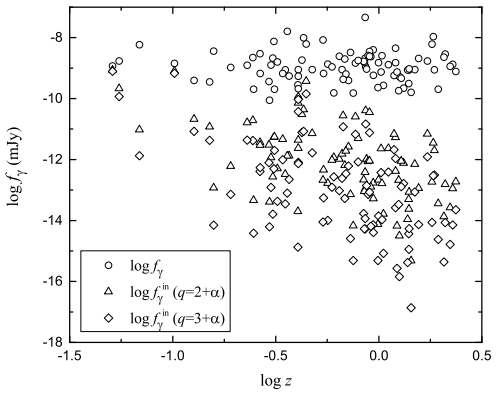

Fig. 1 Plot of γ-ray flux density versus redshift for the whole sample of 91 blazars. Circles stand for observed values, triangles stand for intrinsic values estimated in the case of $q = 2+\alpha$ and rhombuses stand for intrinsic values estimated in the case of $q = 3 + \alpha$.

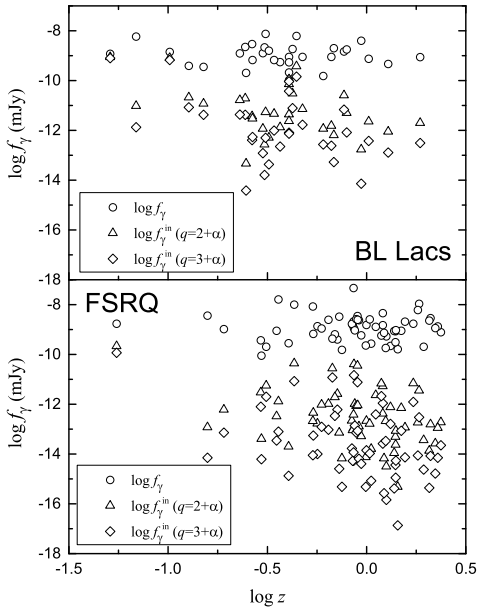

Fig. 2 Plot of γ-ray flux density versus redshift for 32 BL Lacs (*upper panel*) and 59 FSRQs (*lower panel*). Circles stand for observed values, triangles stand for intrinsic values estimated in the case of $q = 2 + \alpha$, and rhombuses stand for intrinsic values estimated in the case of $q = 3 + \alpha$.

with $r = -0.54$ and $p = 5.20 \times 10^{-5}$ for $q = 2+\alpha$; and

$$\log f_\gamma^{\rm in} = -(2.51 \pm 0.55) \log z - (13.75 \pm 0.18)$$

with $r = -0.55$ and $p = 3.40 \times 10^{-5}$ for $q = 3 + \alpha$. The corresponding figure is shown in the lower panel of Figure 3.

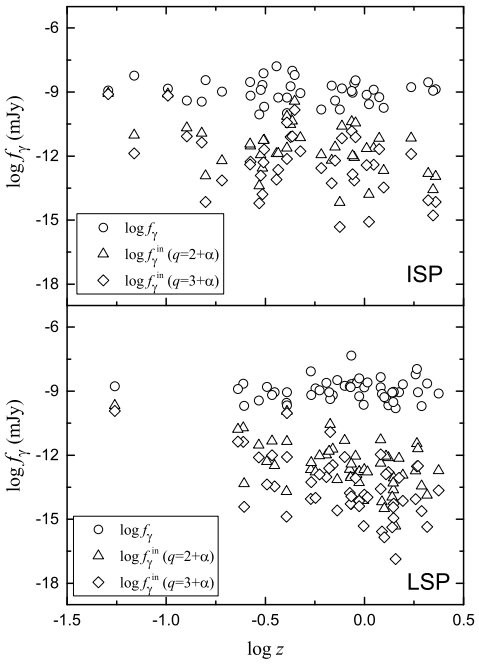

Fig. 3 Plot of γ-ray flux density versus redshift for 40 ISP blazars (*upper panel*) and 51 LSP blazars (*lower panel*). Circles stand for observed values, triangles stand for intrinsic values estimated in the case of $q = 2 + \alpha$, and rhombuses stand for intrinsic values estimated in the case of $q = 3 + \alpha$.

2.3 Short Variability Time Scale and Luminosity

Observations suggest that γ-ray loud blazars are variable on time scales of hours although there is no preferred scale for the variation time of any source (Fan et al. 2014a). For example, *Fermi*/LAT detected a variability time scale of $\sim$12 hours for PKS $1454 - 354$ (Abdo et al. 2009), and a doubling time of roughly four hours for PKS 1502+105 (Abdo et al. 2010b). In the literature, available short variability time scales are collected, e.g., Bassani et al. (1983), Dondi & Ghisellini (1995), Fan et al. (1999b), Gupta et al. (2012) and Vovk & Neronov (2013).

For the sources with available short variability time scales, and X-ray and γ-ray emissions, we can estimate their γ-ray Doppler factors. Following our recent work (Fan et al. 2013a, 2014a), a Doppler factor can be estimated using

$$\delta_\gamma \geq \left[1.54 \times 10^{-3}(1+z)^{4+2\alpha} \left(\frac{d_{\rm L}}{\rm Mpc}\right)^2 \left(\frac{\Delta T}{\rm hr}\right)^{-1} \left(\frac{F_{\rm KeV}}{\mu{\rm Jy}}\right) \left(\frac{E_\gamma}{\rm GeV}\right)^{\alpha}\right]^{\frac{1}{4+2\alpha}},$$

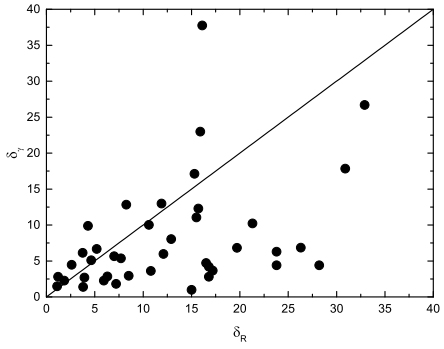

Fig. 4 Plot of γ-ray Doppler factors estimated in this work versus radio Doppler factors from corresponding references.

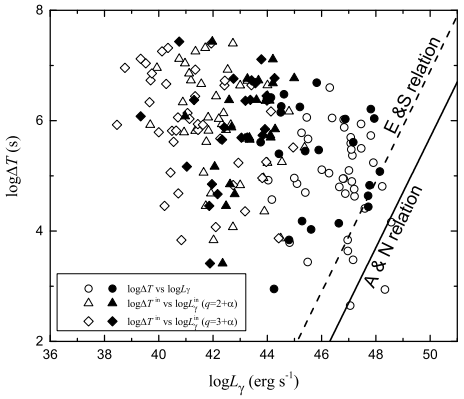

Fig. 5 Plot of short variability time scale versus γ-ray luminosity. Circles stand for observed values, triangles stand for intrinsic values estimated in the case of $q = 2 + \alpha$ and rhombuses stand for intrinsic values estimated in the case of $q = 3 + \alpha$. Filled symbols stand for sources whose intrinsic values are estimated by the γ-ray Doppler factors, while open symbols stand for those by radio Doppler factors.

where ΔT is the variability time scale in units of hours, α is the X-ray spectral index, $F_{\rm keV}$ is the flux density at 1 keV in units of μJy, E_γ is the energy in units of GeV at which the γ-rays are detected, and $d_{\rm L}$ is the luminosity distance in units of Mpc. The average energy E_γ can be calculated by $E_\gamma = \int EdN/\int dN$, and the luminosity distance can be expressed in the form

$$d_{\rm L} = (1+z)\frac{c}{H_0}\int_1^{1+z}\frac{1}{\sqrt{\Omega_M x^3 + 1 - \Omega_M}}\,{\rm d}x$$

from the Λ-CDM model (Capelo & Natarajan 2007) with $\Omega_\Lambda \simeq 0.7$, $\Omega_{\rm M} \simeq 0.3$ and $\Omega_{\rm K} \simeq 0.0$. We adopt $H_0 = 73$ $\rm km\,s^{-1}\,Mpc^{-1}$ throughout the paper. Then, we estimate the γ-ray Doppler factors (δ_γ) of 63 blzazrs and show them in Table 2.

To compare γ-ray Doppler factors estimated in this work with radio Doppler factors, we show the plot of γ-ray Doppler factors versus radio Doppler factors in Figure 4. We find that the γ-ray Doppler factors that we estimated are on average lower than the radio Doppler factors. The reason may be from the fact that the derived value in this work is a lower value as discussed in Fan et al. (2014a).

The luminosity can be calculated using $L_\gamma = 4\pi d_{\rm L}^2(1+z)^{\alpha-1}F_\gamma$, where F_γ is the integral flux calculated by Equation (2) and $(1+z)^{\alpha-1}$ stands for a K-correction into the source rest frame (Fan et al. 2013b; Kapanadze 2013). In a beaming model, the observed photon energy is also beamed, $E^{\rm ob} = \delta E^{\rm in}$, where $E^{\rm in}$ is the intrinsic energy. Because $F = \int f dE$, we have $L^{\rm ob} = \delta^{3+\alpha}L^{\rm in}$ for the case of $q = 2+\alpha$, $L^{\rm ob} = \delta^{4+\alpha}L^{\rm in}$ for the case of $q = 3+\alpha$, and $\Delta T^{\rm in} = \delta\Delta T^{\rm ob}$. Here $L^{\rm in}$ and $\Delta T^{\rm in}$ are the intrinsic luminosity and the intrinsic variability time scale respectively.

For calculating $L_\gamma^{\rm in}$ and $\Delta T^{\rm in}$, we use radio Doppler factors in Table 1, but if there is no available radio Doppler factor, we substitute γ-ray Doppler factors in Table 2 instead. When the Doppler boosting effect is considered, the plot of short variability time scale versus γ-ray luminosity is shown in Figure 5, where both observed properties and intrinsic properties are shown. Then we find that nine blazars violate the E-S or A-N Relation in $L_\gamma^{\rm ob}$ versus $\Delta T^{\rm ob}$. However, the whole sample follows the E-S and A-N Relations in $L_\gamma^{\rm in}$ versus $\Delta T^{\rm in}$, see Figure 5. When the subclasses of blazars are considered, nine FSRQs violate the E-S Relation and three FSRQs violate the A-N Relation in observed data, but all blazars follow those relations in intrinsic data, see Figure 6.

2.4 γ-ray Emissions and Synchrotron Peaked Frequency

For the whole sample of 91 blazars, linear regression analysis is applied to the correlations between γ-ray flux density ($\log f_\gamma$) and synchrotron peak frequency ($\log\nu_{\rm p}^s$). The synchrotron peak frequencies are corrected to the rest frame by $\nu_{\rm p}^{\rm res} = (1+z)\nu_{\rm p}^{\rm obs}$ before analysis.

For $\log f_\gamma$–$\log\nu_{\rm p}^s$ correlation, we have

$$\log f_\gamma = (0.06\pm0.09)\log\nu_{\rm p}^s - (9.75\pm1.21)$$

with $r = 0.07$ and $p = 51.51\%$,

$$\log f_\gamma^{\rm in} = (1.00\pm0.12)\log\nu_{\rm p}^{\rm in} - (25.03\pm1.60)$$

with $r = 0.65$ and $p = 2.54\times10^{-12}$ for $q = 2+\alpha$, and

$$\log f_\gamma^{\rm in} = (1.30\pm0.15)\log\nu_{\rm p}^{\rm in} - (29.84\pm1.95)$$

Table 2 Short Variability Time Scales and γ-ray Doppler Factors for *Fermi* Blazars

3FGL name	Other name	z	Class	$\log \Delta T$	Band	Ref.	F_X	Ref.	α_X	Ref.	F_γ	$\alpha_\gamma^{\rm ph}$	δ_γ
(1)	(2)	(3)	(4)	(5)	(6)	(7)	(8)	(9)	(10)	(11)	(12)	(13)	(14)
J0141.4–0929	1Jy 0138–097	1.034	B	6.03	γ	V13	0.70	LAC	1.15	F14	20.65	2.12	4.45
J0205.0+1510	4C +15.05	0.405	Q	5.78	γ	V13	0.02	BZC	0.37	E14	6.71	2.53	0.99
J0210.7–5101	PKS 0208–512	0.999	Q	5.61	γ	V13	1.62	LAC	1.06	B97	47.40	2.30	5.61
J0222.6+4301	3C 66A	0.444	B	5.10	γ	V13	6.39	LAC	1.60	F14	192.78	1.94	4.46
J0238.6+1636	PKS 0235+164	0.940	B	5.94	γ	V13	1.24	BZC	1.59	F14	103.05	2.17	4.41
J0339.5–0146	PKS 0336–01	0.852	Q	6.02	γ	V13	0.75	BZC	0.62	E14	33.58	2.42	3.67
J0423.2–0119	PKS 0420–01	0.915	Q	5.37	γ	V13	3.87	LAC	0.86	F14	55.92	2.30	6.84
J0442.6–0017	PKS 0440–00	0.844	Q	4.95	γ	V13	4.06	LAC	0.59	E14	34.94	2.50	8.05
J0457.0–2324	PKS 0454–234	1.003	Q	4.83	γ	V13	0.60	BZC	0.48	E14	180.35	2.21	7.31
J0501.2–0157	PKS 0458–02	2.286	Q	5.73	γ	V13	0.92	BZC	0.60	E14	23.24	2.41	12.30
J0510.0+1802	PKS 0507+17	0.416	Q	4.03	γ	L15	0.38	BZC	0.50	E14	13.34	2.41	4.34
J0522.9–3628	PKS 0521–36	0.055	Q	4.57	γ	V13	22.50	LAC	0.92	A09a	47.34	2.44	2.27
J0530.8+1330	PKS 0528+134	2.070	Q	5.24	γ	D95	3.75	LAC	0.58	F14	36.86	2.51	17.83
J0538.8–4405	PKS 0537–441	0.894	B	6.04	γ	V13	4.53	LAC	1.12	F14	329.60	2.04	5.36
J0540.0–2837	1Jy 0537–286	3.104	Q	6.21	γ	V13	1.46	LAC	0.32	F14	7.91	2.78	16.66
J0721.9+7120	1H 0717+714	0.310	B	4.80	γ	V13	4.91	LAC	1.77	F14	219.99	2.04	3.62
J0738.1+1741	PKS 0735+17	0.424	B	6.05	γ	V13	2.09	LAC	1.34	F14	54.82	2.01	2.69
J0739.4+0137	PKS 0736+01	0.191	Q	4.86	Opt	B83	6.36	LAC	0.76	F14	27.34	2.48	2.94
J0831.9+0430	PKS 0829+046	0.230	B	6.06	γ	V13	0.60	BZC	1.00	L16	33.88	2.24	1.40
J0841.4+7053	RBS 0717	2.218	Q	4.41	γ	V13	10.70	LAC	0.42	F14	12.58	2.84	37.76
J0854.8+2006	PKS 0851+202	0.306	B	5.11	γ	V13	1.79	BZC	1.50	F14	59.03	2.18	2.81
J0920.9+4442	S4 0917+44	2.189	Q	5.08	γ	V13	1.83	LAC	0.39	F14	57.84	2.29	19.74
J0957.6+5523	4C +55.17	0.901	Q	5.50	γ	V13	0.77	LAC	0.84	F14	104.50	2.00	5.10
J0958.6+6534	S4 0954+65	0.367	B	5.67	γ	V13	1.12	LAC	0.24	F14	13.81	2.38	2.26
J1104.4+3812	Mkn 421	0.031	B	3.84	X	D95	678.00	LAC	1.82	F14	302.58	1.77	4.13
J1159.5+2914	B2 1156+29	0.729	Q	5.59	γ	V13	1.49	LAC	0.86	F14	83.65	2.21	4.40
J1217.8+3007	1ES 1215+303	0.130	B	4.18	Opt	G12	86.40	LAC	1.47	B00	60.51	1.97	4.66
J1221.4+2814	W Comae	0.102	B	3.79	Opt	F99b	2.29	LAC	1.24	F14	41.23	2.10	2.80
J1224.9+2122	PG 1222+216	0.432	Q	3.64	γ	V13	3.82	LAC	1.19	F14	255.37	2.29	6.68
J1229.1+0202	PKS 1226+02	0.158	Q	4.70	γ	V13	111.00	LAC	1.11	F14	94.24	2.66	4.21
J1256.1–0547	3C 279	0.536	Q	5.48	γ	V13	40.50	LAC	0.84	F14	205.75	2.34	6.29
J1310.6+3222	B2 1308+32	0.997	Q	2.65	Opt	B83	0.85	LAC	0.86	B97a	36.53	2.25	17.12
J1408.8–0751	PKS B1406–076	1.494	Q	4.76	γ	F99a	0.53	BZC	0.07	F13	17.90	2.38	12.84
J1439.2+3931	PG 1437+398	0.344	B	6.25	γ	V13	17.90	LAC	1.33	F14	4.44	1.77	3.25
J1457.4–3539	PKS 1454–354	1.424	Q	4.64	γ	A09b	0.51	BZC	0.68	E14	66.18	2.29	10.41
J1504.4+1029	PKS 1502+106	1.839	Q	4.16	γ	A10	0.16	BZC	0.84	F14	239.96	2.24	12.98
J1512.8–0906	PKS 1510–089	0.360	Q	3.84	γ	V13	1.15	BZC	0.98	F14	411.05	2.36	4.73
J1517.6–2422	AP Librae	0.049	B	2.95	Opt	B83	2.92	LAC	1.36	F14	52.34	2.11	2.89
J1535.0+3721	RGB J1534+372	0.143	B	6.42	γ	V13	0.37	LAC	1.84	F14	4.10	2.11	1.07
J1540.8+1449	PKS 1538+149	0.605	B	3.44	Opt	F96	1.82	LAC	0.66	F14	3.70	2.34	9.88
J1626.0–2951	PKS 1622–297	0.815	Q	4.14	γ	M97	2.28	LAC	0.45	E14	25.02	2.45	10.66
J1635.2+3809	B3 1633+382	1.814	Q	4.81	γ	V13	0.17	BZC	0.62	F14	114.44	2.40	10.22
J1642.9+3950	3C 345	0.593	Q	5.05	Opt	D95	4.07	LAC	0.81	F14	25.12	2.45	5.37
J1653.9+3945	Mkn 501	0.034	B	5.40	Inf	B83	65.10	LAC	1.36	F14	97.38	1.72	1.96
J1728.3+5013	I Zw 187	0.055	B	5.61	X	B83	39.60	LAC	1.39	F14	10.81	1.96	1.86
J1733.0–1305	PKS 1730–130	0.902	Q	4.90	γ	V13	6.32	LAC	0.50	F14	55.89	2.35	10.02
J1740.3+5211	S4 1739+52	1.379	Q	5.70	γ	V13	1.25	LAC	1.08	F14	16.66	2.45	6.85
J1748.6+7005	S4 1749+70	0.770	B	4.68	γ	V13	1.55	LAC	1.44	F14	41.38	2.06	6.14
J1751.5+0939	OT 081	0.322	B	5.47	γ	V13	1.18	BZC	0.74	L15	42.51	2.25	2.39
J1800.5+7827	S5 1803+78	0.684	B	4.95	γ	V13	1.71	LAC	0.45	F14	50.65	2.22	5.97
J1806.7+6949	3C 371	0.051	B	4.92	Opt	B83	4.79	LAC	0.75	F14	33.48	2.23	1.49
J1813.6+3143	B2 1811+31	0.117	B	6.26	γ	V13	1.44	LAC	2.60	L15	15.44	2.12	1.27
J1824.2+5649	S4 1823+56	0.664	B	6.60	γ	V13	2.52	LAC	0.96	F14	20.11	2.46	2.86

Table 2 — *Continued.*

3FGL name	Other name	z	Class	$\log \Delta T$	Band	Ref.	F_X	Ref.	α_X	Ref.	F_γ	$\alpha_\gamma^{\rm ph}$	δ_γ
(1)	(2)	(3)	(4)	(5)	(6)	(7)	(8)	(9)	(10)	(11)	(12)	(13)	(14)
J1833.6–2103	PKS 1830–210	2.507	Q	4.44	γ	V13	3.25	LAC	0.13	F14	15.44	2.12	43.49
J2009.3–4849	1Jy 2005–489	0.071	B	6.48	γ	V13	80.80	LAC	1.32	F14	35.54	1.77	1.78
J2134.1–0152	PKS 2131–021	1.285	B	5.88	γ	V13	0.67	LAC	1.05	F14	11.18	2.21	5.66
J2143.5+1744	S3 2141+17	0.211	Q	5.45	γ	V13	1.76	LAC	1.44	F14	44.18	2.52	1.92
J2158.8–3013	PKS 2155–304	0.117	B	6.69	γ	V13	572.00	LAC	1.62	F14	216.84	1.83	2.64
J2202.7+4217	B3 2200+420	0.069	B	4.96	γ	V13	7.42	LAC	0.83	F14	164.77	2.25	1.81
J2225.8–0454	3C 446	1.404	Q	3.48	Opt	B83	2.12	LAC	0.59	F14	19.43	2.36	22.99
J2232.5+1143	PKS 2230+11	1.037	Q	4.63	Opt	B83	3.06	LAC	0.51	F14	50.19	2.52	11.05
J2250.1+3825	B3 2247+381	0.119	B	6.15	γ	V13	7.93	LAC	1.51	F14	11.02	1.91	1.69
J2254.0+1608	PKS 2251+15	0.859	Q	2.94	γ	V13	19.00	LAC	0.62	F14	1060.92	2.35	26.71

Note: Column (1) gives the *Fermi* name; Col. (2) other name; Col. (3) redshift; Col. (4) classification, "B" stands for BL Lacs and "Q" stands for FSRQs; Col. (5) short variability time scale ($\log \Delta T$) in units of s; Col. (6) band at which ΔT is detected; Col. (7) references for Cols. (3), (5) and (6); Cols. (8) and (9) X-ray flux in units of 10^{-12} erg cm^{-2} s^{-1} at 0.1–2.4 keV and its reference respectively; Cols. (10) and (11) X-ray spectral index and its reference respectively; Cols. (12) and (13) γ-ray integral photon flux at 1–100 GeV in units of 10^{-10} ph cm^{-2} s^{-1} and photon spectrum index ($\alpha_\gamma^{\rm ph}$) from 3LAC respectively; Col. (14) γ-ray Doppler factor (δ_γ). Here, LAC: Ackermann et al. 2015; BZC: Massaro et al. (2015); A09a: Ajello et al. (2009); A09b: Abdo et al. (2009); A10: Abdo et al. (2010b); B83: Bassani et al. (1983); B97: Brinkmann et al. (1997); B00: Brinkmann et al. (2000); D95: Dondi & Ghisellini (1995); E14: Evans et al. (2014); F96: Fan & Lin (1996); F99a: Fan et al. (1999b); F99b: Fan et al. (1999a); F09: Fan et al. (2009); F13: Fan et al. (2013a); F14: Fan et al. (2014a); G12: Gupta et al. (2012); H09: Hovatta et al. (2009); LB15: Liao & Bai (2015); LF16: Lin & Fan (2016); LV99: Lähteenmäki & Valtaoja (1999); M97: Mattox et al. (1997); S10: Savolainen et al. (2010); V13: Vovk & Neronov (2013). If a source has short variability time scales in different references, the value in the latest one is considered.

with $r = 0.68$ and $p = 1.97 \times 10^{-13}$ for $q = 3 + \alpha$; here $\nu_{\rm p}^{\rm in} = \nu_{\rm p}^{\rm res}/\delta$ is an intrinsic peak frequency. The corresponding figure is shown in Figure 7.

As results show in Section 2.2 and in Lin & Fan (2016), γ-ray flux density is strongly correlated with redshift, therefore the correlations between γ-ray emissions and peak frequency may be caused by a redshift effect. In our recent works (Fan et al. 2013b; Fan et al. 2015a; Lin & Fan 2016), we have removed the redshift effect from the luminosity-luminosity correlation by using the partial correlation introduced by Padovani (1992). If variables i and j are correlated with a third one k, then the correlation between i and j can remove the k effect, as follows:

$$r_{ij,k} = (r_{ij} - r_{ik}r_{jk})/\sqrt{(1 - r_{ik}^2)(1 - r_{jk}^2)},$$

where r_{ij}, r_{ik} and r_{jk} are the correlation coefficients between any two variables of i, j and k respectively. When the method is applied to the

$$\log f_\gamma^{\rm in} - \log \nu_{\rm p}^{\rm in}$$

correlation, the correlation coefficients excluding the redshift effect for the whole sample are as follows: $r_{f\nu,z}$ = 0.56 with $p_{f\nu,z} = 8.09 \times 10^{-9}$ for $q = 2 + \alpha$ and $r_{f\nu,z}$ = 0.59 with $p_{f\nu,z} = 7.52 \times 10^{-10}$ for $q = 3 + \alpha$.

3 DISCUSSION AND CONCLUSIONS

In this work, we collect 91 blazars with available radio Doppler factors, and calculate their intrinsic γ-ray flux density ($\log f_\gamma^{\rm in}$) at 2 GeV and intrinsic synchrotron peak frequency ($\log \nu_{\rm p}^{\rm in}$). Then the correlations between $\log f_\gamma^{\rm in}$ and redshift, and between $\log f_\gamma^{\rm in}$ and $\log \nu_{\rm p}^{\rm in}$ are investigated. We also study the intrinsic relation between short variability time scale ($\Delta T^{\rm in}$) and γ-ray luminosity ($\log L_\gamma^{\rm in}$) for 63 blazars by comparing to the E-S and A-N Relations.

In our recent work, we compared the γ-ray Doppler factors (δ_γ) with the radio Doppler factors (δ_R), and found they are associated with each other, see Fan et al. (2014a). So, we can investigate the beaming effect in the γ-ray band by using the radio Doppler factors. We also found that the radio Doppler factor correlates well with γ-ray luminosity for the *Fermi* detected sources, see Fan et al. (2009). In this work, we find that values of $\log f_\gamma^{\rm in}$ of FSRQs are smaller than those of BL Lacs with a probability for the two groups to come from the same distribution (Kolmogorov-Smirnov (K-S) test) being $p < 10^{-5}$ for $q = 2 + \alpha$ and $q = 3 + \alpha$. The averaged values of $\log f_\gamma^{\rm in}$ are

$$\langle \log f_\gamma^{\rm in} \rangle = -12.52 \pm 1.12 \ \ (q = 2 + \alpha),$$

$$\langle \log f_\gamma^{\rm in} \rangle = -13.56 \pm 1.38 \ \ (q = 3 + \alpha)$$

for FSRQs; and

$$\langle \log f_\gamma^{\rm in} \rangle = -11.25 \pm 1.00 \ \ (q = 2 + \alpha),$$

$$\langle \log f_\gamma^{\rm in} \rangle = -11.95 \pm 1.29 \ \ (q = 3 + \alpha)$$

for BL Lacs. A t-test indicates that the averaged difference of $\log f_\gamma^{\rm in}$ between BL Lacs and FSRQs is

$$\Delta(\log f_\gamma^{\rm in}) = 1.27 \pm 0.24$$

with a significance level of $p < 10^{-6}$ for $q = 2 + \alpha$, and $\Delta(\log f_\gamma^{\rm in}) = 1.61 \pm 0.30$ with $p < 10^{-6}$ for $q = 3 + \alpha$, while the averaged difference of the observed flux density ($\log f_\gamma$) is $\Delta(\log f_\gamma) = 0.05 \pm 0.11$ with $p = 64.23\%$.

3.1 γ-ray Flux Density and Redshift

We analyze the whole sample of 91 *Fermi* blazars, and find that $\log f_\gamma$ is weakly correlated with redshift ($r = -0.01$, and slope is -0.01 ± 0.15). The result is different from our expectation: $\log f = -2.0 \log z + {\rm const}$, if blazars belong to a group. But when we consider the strong beaming effect of γ-ray emissions for *Fermi* blazars, we find that $\log f_\gamma^{\rm in}$ is strongly correlated with redshift as follows: $\log f_\gamma^{\rm in} = -(1.82 \pm 0.30) \log z - (12.44 \pm 0.13)$ with $r = -0.54$ and $p = 2.98 \times 10^{-8}$ for $q = 2 + \alpha$, and $\log f_\gamma^{\rm in} = -(2.32 \pm 0.37) \log z - (13.46 \pm 0.16)$ with $r = -0.55$ and $p = 1.66 \times 10^{-8}$ for $q = 3 + \alpha$. In our recent work (Xiao et al. 2015), we found that $\log f_\gamma^{\rm in}$ and redshift have a strong correlation ($p < 10^{-4}$) with the slopes being -2.05 ± 0.32 ($q = 2 + \alpha$) and -2.55 ± 0.34 ($q = 3 + \alpha$) respectively. Results in the present work suggest that $\log f_\gamma^{\rm in}$ and redshift follow the theoretical relation, which is consistent with our previous work (Xiao et al. 2015).

For subclasses of blazars, some similar correlation results are found, but their slopes are slightly different. The slopes of correlations between $\log f_\gamma^{\rm in}$ and redshift are -1.30 ± 0.47 (BL Lacs), -1.34 ± 0.45 (FSRQs), -1.33 ± 0.44 (ISP) and -1.95 ± 0.44 (LSP) for the case of $q = 2 + \alpha$; and those are -1.65 ± 0.61 (BL Lacs), -1.73 ± 0.55 (FSRQs), -1.67 ± 0.54 (ISP) and -2.51 ± 0.55 (LSP) for $q = 3 + \alpha$. In our results, slopes of BL Lacs are very close to those of FSRQs, and they favor the jet case of $q = 3 + \alpha$. However, for the whole sample, the results of slopes indicate that two jet cases exist in blazars, since slopes are -1.82 ± 0.30 for $q = 2 + \alpha$, -2.32 ± 0.37 for $q = 3 + \alpha$, and ~ -2.0 for the theoretical relation. For the SED classification, results of slopes suggest that ISP blazars favor the jet case of $q = 3 + \alpha$, while LSP blazars favor the jet case of $q = 2 + \alpha$. Those results indicate stationary jets ($q = 2 + \alpha$) are perhaps dominant in LSP blazars. A possible explanation of those results is the differences in synchrotron peaked frequency caused by the physical differences in blazars, such as the different forms of relativistic jets. In Xiao et al. (2015), we suggested that the continuous case ($q = 2 + \alpha$) of a jet is perhaps real for *Fermi* blazars, however, we did not discuss the subclasses in that work. In the present work, we cannot discuss this further since there is no Doppler factor for HSP blazars.

3.2 Short Variability Time Scale and Luminosity

For the whole sample of 63 blazars, our results show that nine blazars violate the E-S or A-N Relation in $L_\gamma^{\rm ob}$ versus $\Delta T^{\rm ob}$, but the whole sample follows the E-S and A-N Relations in $L_\gamma^{\rm in}$ versus $\Delta T^{\rm in}$, see Figures 5 and 6.

In our recent work (Xiao et al. 2015), some similar results are found for a sample of 28 blazars. Different subclasses of blazars have different properties, for instance FSRQs have strong emission lines, so that their redshifts can be determined more easily and accurately than those of BL Lacs, and FSRQs statistically have higher redshift and lower synchrotron peaked frequency than BL Lacs. Therefore, for further analysis, the subclasses of blazars are considered. We find that nine FSRQs violate the E-S Relation and three FSRQs violate the A-N Relation in $L_\gamma^{\rm ob}$ versus $\Delta T^{\rm ob}$, but all blazars follow those relations in their intrinsic properties. In addition, the averaged values of radio Doppler factors are $\langle \delta_{\rm R} \rangle = 6.50 \pm 4.87$ for 32 BL Lacs and $\langle \delta_{\rm R} \rangle = 13.47 \pm 8.04$ for 59 FSRQs. From a K-S test, the probability that the distributions of δ_R for BL Lacs and FSRQs are drawn from the same parent distribution is $p = 6.87 \times 10^{-5}$. Thus, the Doppler factors of FSRQs are larger than those of BL Lacs, which is consistent with our previous result (Fan et al. 2004). From the above analysis, we find that the beaming effect is an important reason that causes blazars to violate the E-S and A-N Relations, and FSRQs have a stronger beaming effect than BL Lacs.

3.3 γ-ray Emissions and Synchrotron Peaked Frequency

There is no correlation between $\log f_\gamma$ and $\log \nu_{\rm p}^{\rm s}$ with $r = 0.07$ and $p = 51.51\%$. However, strong positive correlations are found between $\log f_\gamma^{\rm in}$ and $\log \nu_{\rm p}^{\rm in}$ for the whole sample. Those correlation coefficients and chance probabilities are $r = 0.65$ and $p = 2.54 \times 10^{-12}$ for the case of $q = 2 + \alpha$, and $r = 0.68$ and $p = 1.97 \times 10^{-13}$ for $q = 3 + \alpha$ respectively. When the redshift effect is removed, strong positive correlations still exist between them. In Lister et al. (2011), strong anti-correlations are found between observed radio flux density at 5 GHz and synchrotron peak frequency for BL Lacs and FSRQs. From results in Lister et al. (2011) and this work, the anti-correlations (or no correlation) between observed

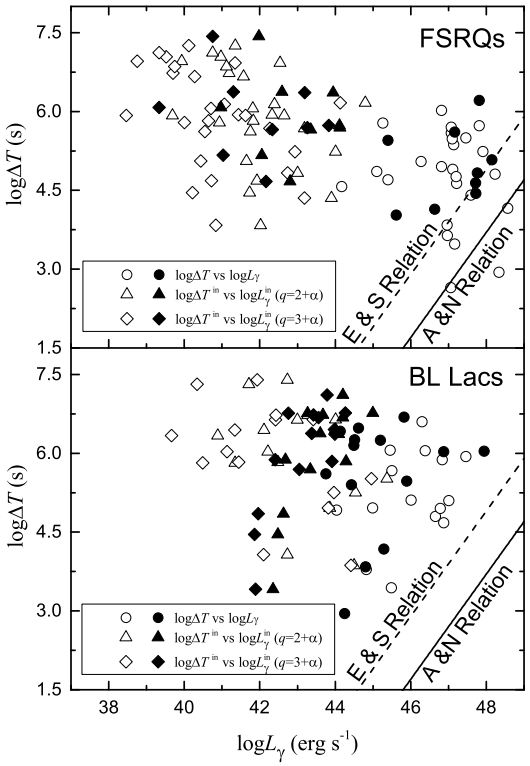

Fig. 6 Plot of short variability time scale versus γ-ray luminosity for 31 FSRQs (*upper panel*) and 26 BL Lacs (*lower panel*). Circles stand for observed values, triangles stand for intrinsic values estimated in the case of $q = 2 + \alpha$, and rhombuses stand for intrinsic values estimated in the case of $q = 3 + \alpha$. Filled symbols stand for sources whose intrinsic values are estimated by γ-ray Doppler factors, while open symbols stand for those by radio Doppler factors.

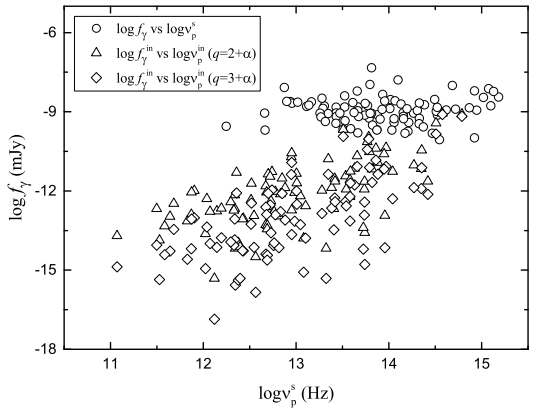

Fig. 7 Plot of γ-ray flux density versus synchrotron peak frequency for the whole sample of 91 blazars. Circles stand for observed values, triangles stand for intrinsic values estimated in the case of $q = 2 + \alpha$, and rhombuses stand for intrinsic values estimated in the case of $q = 3 + \alpha$.

flux densities and synchrotron peak frequency are significantly different from the positive correlations in intrinsic properties. Thus, the beaming effect cannot be ignored when we investigate the physical mechanism of blazars.

The blazar sequence, which is defined by the anti-correlation between peak luminosity and peak frequency, can be explained by the cooling effect (Fossati et al. 1998; Ghisellini et al. 1998; Wu et al. 2007; Nieppola et al. 2008). However, that theoretical explanation of the blazar sequence does not consider the beaming effect. Therefore, the intrinsic correlation between peak luminosity and peak frequency is needed to investigate the blazar sequence. Wu et al. (2007) estimated Doppler factors (δ) for a sample of 170 BL Lacs and found significant anti-correlations between δ and $\nu_{\rm p}^{\rm in}$, and between the total 408 MHz luminosity ($L_{408\,\rm MHz}$) and $\nu_{\rm p}^{\rm in}$. However, the scatter of $L_{408\,\rm MHz}$ versus $\nu_{\rm p}^{\rm in}$ is very large, which is in contrast with the much tighter relation of blazar sequence. Some similar results are found between radio power and $\nu_{\rm p}^{\rm s}$ in Nieppola et al. (2006). Recently, some high-luminosity high-$\nu_{\rm p}^{\rm s}$ and low-luminosity low-$\nu_{\rm p}^{\rm s}$ sources have been detected. Those results indicate that the blazar sequence is likely to be eliminated (Wu et al. 2007).

Nieppola et al. (2008), who collected a sample of 89 AGNs with available Doppler factors, found strong anti-correlation between δ and $\nu_{\rm p}^{\rm in}$, and proposed that the lower peak frequency blazars are more boosted. In Nieppola et al. (2008), a positive Spearman rank correlation between intrinsic synchrotron peak luminosity ($L_{\rm p}^{\rm in}$) and $\nu_{\rm p}^{\rm in}$ was also found with $r = 0.366$ and $p = 3 \times 10^{-3}$ for blazars, especially for BL Lacs ($r = 0.642$ and $p < 10^{-3}$). They concluded that the anti-correlation between $L_{\rm p}^{\rm in}$ and $\nu_{\rm p}^{\rm in}$ which is used to determine the blazar sequence is not present, suggesting that the blazar sequence is an artifact of variable Doppler boosting across the peak frequency range. However, scatter in the correlation between $L_{\rm p}^{\rm in}$ and $\nu_{\rm p}^{\rm in}$ is about five orders of magnitude for their sample. In addition, Wu et al. (2009) found a significant positive $L_{\rm p}^{\rm in}$–$\nu_{\rm p}^{\rm in}$ correlation with a Spearman correlation coefficient of $r = 0.59$ at the $> 99.99\%$ confidence level. In this work, we find a positive correlation between $\log f_{\gamma}^{\rm in}$ and $\log \nu_{\rm p}^{\rm in}$ after correcting the redshift effect. Thus, our results and previous research indicate that there is a positive correlation between intrinsic emissions and intrinsic synchrotron peak frequency.

Interestingly, we find a strong positive correlation between $\nu_{\rm p}^{\rm in}$ and $\nu_{\rm p}^{\rm s}$: $\log \nu_{\rm p}^{\rm in} = (1.19 \pm 0.06) \log \nu_{\rm p}^{\rm s} - (3.58 \pm 0.79)$ with $r = 0.91$ and $p = 2.13 \times 10^{-36}$. The strong positive $\nu_{\rm p}^{\rm in}$–$\nu_{\rm p}^{\rm s}$ correlation indicates that there is almost no difference in the order of blazars along the peak frequency between before and after considering the beaming effect. Thus, intrinsic properties of the blazar order would not be eliminated, although the relation between luminosity and peak frequency is changed significantly. The observed blazar order is strongly associated with the intrinsic one. Therefore, a new theoretical explanation is needed for the intrinsic blazar order. In addition, we noticed that the intrinsic blazar order could change what we know about blazars, such as differences in black hole mass between BL Lacs and FSRQs.

The positive correlation between γ-ray emissions and peak frequency indicates that the synchrotron emissions are highly correlated with γ-ray emissions. From the synchrotron self-Compton (SSC) process, γ-ray emissions are produced by the inverse Compton scattering process from synchrotron emissions, so that they should be associated with each other. In addition, we suppose that $f_{\gamma}^{\rm in} - \nu_{\rm p}^{\rm in}$ and $\nu_{\rm p}^{\rm in} - \nu_{\rm p}^{\rm s}$ relations can be used to estimate the Doppler boosting factors. However, a larger sample is needed to find more accurate correlations.

3.4 Conclusions

In this work, we collect 91 *Fermi* blazars with available Doppler factors, and investigate the correlations between intrinsic flux density and redshift for the whole sample, BL Lacs, FSRQs, ISP and LSP separately. Then, we estimate γ-ray Doppler factors of 63 blazars, and study the relationship between γ-ray luminosity and short variability time scale for those blazars. The observed and intrinsic correlations between the γ-ray flux density and synchrotron peak frequency are also investigated for the whole blazar sample. Our main conclusions are as follows:

(1) The correlation between $f_{\gamma}^{\rm in}$ and redshift follows the theoretical relation: $\log f = -2.0 \log z + \rm const.$ When the subclasses are considered, we find that the stationary jets are perhaps dominant in LSP blazars.
(2) Nine FSRQs violate the E-S or A-N Relation in $L_{\gamma}^{\rm ob}$ versus $\Delta T^{\rm ob}$, while the whole blazar sample obeys the E-S and A-N Relations in $L_{\gamma}^{\rm in}$ versus $\Delta T^{\rm in}$. Thus, FSRQs have a stronger beaming effect than BL Lacs.
(3) Strong positive correlation between $f_{\gamma}^{\rm in}$ and $\nu_{\rm p}^{\rm in}$ is found, which suggests that synchrotron emissions are highly correlated with γ-ray emissions.

Acknowledgements This work is supported by the National Natural Science Foundation of China (Grant Nos. U1531245, U1431112, 11203007, 11403006, 10633010, 11173009 and 11403006), and the Innovation

Foundation of Guangzhou University (IFGZ), Guangdong Innovation Team (2014KCXTD014), Guangdong Province Universities and Colleges Pearl River Scholar Funded Scheme (GDUPS) (2009), Yangcheng Scholar Funded Scheme (10A027S), and support for Astrophysics Key Subjects of Guangdong Province and Guangzhou City.

References

Abdo, A. A., Ackermann, M., Atwood, W. B., et al. 2009, ApJ, 697, 934

Abdo, A. A., Ackermann, M., Ajello, M., et al. 2010a, ApJS, 188, 405

Abdo, A. A., Ackermann, M., Ajello, M., et al. 2010b, ApJ, 710, 810

Abdo, A. A., Ackermann, M., Agudo, I., et al. 2010c, ApJ, 716, 30

Abramowicz, M. A., & Nobili, L. 1982, Nature, 300, 506

Acero, F., Ackermann, M., Ajello, M., et al. 2015, ApJS, 218, 23

Ackermann, M., Ajello, M., Allafort, A., et al. 2011, ApJ, 743, 171

Ackermann, M., Ajello, M., Atwood, W. B., et al. 2015, ApJ, 810, 14

Ajello, M., Costamante, L., Sambruna, R. M., et al. 2009, ApJ, 699, 603

Bassani, L., Dean, A. J., & Sembay, S. 1983, A&A, 125, 52

Brinkmann, W., Yuan, W., & Siebert, J. 1997, A&A, 319, 413

Brinkmann, W., Laurent-Muehleisen, S. A., Voges, W., et al. 2000, A&A, 356, 445

Capelo, P. R., & Natarajan, P. 2007, New Journal of Physics, 9, 445

Catanese, M., & Weekes, T. C. 1999, PASP, 111, 1193

Cheng, K. S., Fan, J. H., & Zhang, L. 1999, A&A, 352, 32

Cheng, K. S., Zhang, X., & Zhang, L. 2000, ApJ, 537, 80

Chen, Y. Y., Zhang, X., Zhang, H. J., & Yu, X. L. 2015, MNRAS, 451, 4193

Chen, Y.-Y., Zhang, X., Xiong, D.-R., Wang, S.-J., & Yu, X.-L. 2016, RAA (Research in Astronomy and Astrophysics), 16, 13

Dondi, L., & Ghisellini, G. 1995, MNRAS, 273, 583

Elliot, J. L., & Shapiro, S. L. 1974, ApJ, 192, L3

Evans, P. A., Osborne, J. P., Beardmore, A. P., et al. 2014, ApJS, 210, 8

Fan, J., & Lin, R. 1996, Publications of the Yunnan Observatory, 4, 8

Fan, J. H., Adam, G., Xie, G. Z., et al. 1998, A&A, 338, 27

Fan, J., Feng, X., & Su, C. 1999a, Publications of the Yunnan Observatory, 2, 1

Fan, J. H., Xie, G. Z., & Bacon, R. 1999b, A&AS, 136, 13

Fan, J.-H., Wang, Y.-J., Yang, J.-H., & Su, C.-Y. 2004, ChJAA (Chin. J. Astron. Astrophys.), 4, 533

Fan, J. H. 2005, A&A, 436, 799

Fan, J.-H., Huang, Y., He, T.-M., et al. 2009, PASJ, 61, 639

Fan, J.-H., Yang, J.-H., Liu, Y., & Zhang, J.-Y. 2013a, RAA (Research in Astronomy and Astrophysics), 13, 259

Fan, J., Yang, J. H., Zhang, J.-Y., et al. 2013b, PASJ, 65, 25

Fan, J.-H., Bastieri, D., Yang, J.-H., et al. 2014a, RAA (Research in Astronomy and Astrophysics), 14, 1135

Fan, J. H., Bastieri, D., Yang, J. H., et al. 2014b, Journal of Astrophysics and Astronomy, 35, 231

Fan, J. H., & Ji, Z. Y. 2014, in IAU Symposium, 304, Multiwavelength AGN Surveys and Studies, ed. A. M. Mickaelian & D. B. Sanders, 159

Fan, J. H., Yang, J. H., Liu, Y., et al., 2015a, IJMPA, 3045020F, *http://cdsads.u-strasbg.fr/abs/2015IJMPA..3045020F*

Fan, J. H., Xiao, H. B., Bastieri, D., et al. 2015b, in IAU Symposium, 313, Extragalactic Jets from Every Angle, ed. F. Massaro, C. C. Cheung, E. Lopez, & A. Siemiginowska, 53

Fan, J. H., Yang, J. H., Liu, Y., et al. 2016, ApJS, 226, 20

Fossati, G., Maraschi, L., Celotti, A., Comastri, A., & Ghisellini, G. 1998, MNRAS, 299, 433

Ghisellini, G., Celotti, A., Fossati, G., Maraschi, L., & Comastri, A. 1998, MNRAS, 301, 451

Ghisellini, G., Padovani, P., Celotti, A., & Maraschi, L. 1993, ApJ, 407, 65

Gupta, S. P., Pandey, U. S., Singh, K., et al. 2012, New Astron., 17, 8

Holder, J. 2012, Astroparticle Physics, 39, 61

Hovatta, T., Valtaoja, E., Tornikoski, M., & Lähteenmäki, A. 2009, A&A, 494, 527

Jorstad, S. G., Marscher, A. P., Mattox, J. R., et al. 2001a, ApJ, 556, 738

Jorstad, S. G., Marscher, A. P., Mattox, J. R., et al. 2001b, ApJS, 134, 181

Kapanadze, B. Z. 2013, AJ, 145, 31

Kellermann, K. I., Lister, M. L., Homan, D. C., et al. 2004, ApJ, 609, 539

Lähteenmäki, A., & Valtaoja, E. 1999, ApJ, 521, 493

Lähteenmäki, A., & Valtaoja, E. 2003, ApJ, 590, 95

Li, B., Zhang, H., Zhang, X., et al. 2013, Ap&SS, 347, 349

Liao, N. H., & Bai, J. M. 2015, New Astron., 34, 134

Lin, C., & Fan, J.-H. 2016, RAA (Research in Astronomy and Astrophysics), 16, 103

Lister, M. L., Homan, D. C., Kadler, M., et al. 2009, ApJ, 696, L22

Lister, M. L., Aller, M., Aller, H., et al. 2011, ApJ, 742, 27
Massaro, E., Maselli, A., Leto, C., et al. 2015, Ap&SS, 357, 75
Mattox, J. R., Wagner, S. J., Malkan, M., et al. 1997, ApJ, 476, 692
Nieppola, E., Tornikoski, M., & Valtaoja, E. 2006, A&A, 445, 441
Nieppola, E., Valtaoja, E., Tornikoski, M., Hovatta, T., & Kotiranta, M. 2008, A&A, 488, 867
Nolan, P. L., Abdo, A. A., Ackermann, M., et al. 2012, ApJS, 199, 31
Padovani, P. 1992, A&A, 256, 399
Pei, Z.-Y., Fan, J.-H., Liu, Y., et al. 2016, Ap&SS, 361, 237
Ruan, J. J., Anderson, S. F., Plotkin, R. M., et al. 2014, ApJ, 797, 19
Savolainen, T., Homan, D. C., Hovatta, T., et al. 2010, A&A, 512, A24
Valtaoja, E., & Terasranta, H. 1995, A&A, 297, L13
Vovk, I., & Neronov, A. 2013, ApJ, 767, 103
Weekes, T. C. 1997, in Bulletin of the American Astronomical Society, 29, American Astronomical Society Meeting Abstracts, 1264
Wu, D.-X., Fan, J.-H., Liu, Y., et al. 2014, PASJ, 66, 117
Wu, Z., Jiang, D. R., Gu, M., & Liu, Y. 2007, A&A, 466, 63
Wu, Z.-Z., Gu, M.-F., & Jiang, D.-R. 2009, RAA (Research in Astronomy and Astrophysics), 9, 168
Xiao, H.-B., Pei, Z.-Y., Xie, H.-J., et al. 2015, Ap&SS, 359, 39
Xie, G. Z., Zhang, Y. H., & Fan, J. H. 1997, ApJ, 477, 114
Xiong, D., Zhang, H., Zhang, X., et al. 2013, Ap&SS, 343, 345
Yang, J. H., Fan, J. H., Hua, T. X., & Wu, D. X. 2014, Ap&SS, 352, 819
Zhang, J., Liang, E.-W., Zhang, S.-N., & Bai, J. M. 2012, ApJ, 752, 157
Zhang, J.-S., & Fan, J.-H. 2003, ChJAA (Chin. J. Astron. Astrophys.), 3, 415